Selective Hydrolysis by Engineered Cutinases: Characterization of Aliphatic-aromatic Polyester Homo and Co-polymers by LC and LC-MS Methods

Eman Abdelraheem[+a], Vasilis Tseliou[+a], Jessica Desport[a], Martin Schürmann[b], Paul Buijsen[c], Ron Peters[a,c], Andrea F. G. Gargano*[a], Francesco G. Mutti*[a]

The performance, biodegradability, and recyclability of polymers can be tuned during synthesis by adopting monomers with different chemical characteristics. Recent research has shown the aptness of some hydrolases to depolymerize polyesters under mild conditions compared to chemical approaches. Herein, we engineered a cutinase from *Thermobifida cellulosilytica* (Tc_Cut2NV^{WCCG}) for improved thermostability (up to 91 °C) and compared it with previously reported leaf-branch compost cutinase (LCC^{WCCG}) for the hydrolysis of oligomers, aliphatic and aromatic polyester homopolymers, and a co-polyester. For both enzymes, higher hydrolysis rates were observed for aliphatic compared to aromatic homopolyesters. SEC-MS analysis revealed that the hydrolysis of aliphatic/aromatic co-polyesters occurred at the aliphatic monomers, significantly reducing the molecular weight and changing the end-group composition. These results underline the importance of co-polymer composition in the biodegradation of co-polymer systems and highlight the potential use of enzymes for the analytical characterization of synthetic polymers by selectively reducing their molecular weight.

Introduction

The chemical composition of polymers (i.e., types of end groups, co-polymer ratio, molecular weight) is an important parameter for determining their mechanical properties, including degradability and melting point.[1-10] A detailed understanding of polymer composition is pivotal to designing materials that offer improved recyclability and controlled biodegradation.[11] Therefore, the development of catalytic methods that enable controlled polymer depolymerization is of high interest for applications in polymer recycling and analytical chemistry that aim to characterize polymer distribution. The physical and chemical degradation of polymers includes thermal, photochemical, mechanochemical, and oxidating processes.[12-14] These processes can successfully degrade the polymer but lack selectivity.

In contrast, enzymes offer the potential for chemoselective degradation of polymers by targeting specific bonds. Moreover, enzymes can display different hydrolytic kinetics for different monomers depending on the neighboring monomer within the polymer sequence. Therefore, available and novel hydrolases could be applied to characterize the microstructure of synthetic polymers similarly to what is done for the characterization of proteins (i.e., chemoselective digestion).

The capability of some hydrolases to degrade synthetic polyesters has been investigated over the past two decades, leading to the discovery and engineering of variants that can fully degrade polyethylene terephthalate (PET) and, therefore, potentially be used for recycling and bioremediation purposes. The enzymes used for this purposes were cutinases isolated from microbial strains (e.g. *Ideonella sakaiensis* and *Thermobifida fusca*) or fungi (*Fusarium solani*, *Humicola insolens*, and *Aspergillus oryzae*), and further engineered.[15-20] Among the recently published candidates enzymes for PET hydrolysis are *Thermobifida fusca* cutinase (TfCut2)[21, 22], *Thermobifida cellulosilytica* cutinase 1 (ThcCut1)[23] and an engineered leaf-branch compost cutinase (LCC^{WCCG}).[24] Further recent research has also led to the discovery and engineering of other catalytically active and thermostable enzymes for the depolymerization of PET.[25-36]

However, these recent works on polyester degradation by enzymes has mainly focused on methods to degrade homopolymers back to the starting monomers. Müller et al. have studied the process of co-polyesters hydrolysis, revealing that the cleavage rates are dependent on the heterogeneity of the polymer as well as the chemical structure and molecular environment (crystallinity) in which the ester bonds are embedded.[37-41] Yet, to date, analytical investigations studying the changes of chemical structures in co-polymers as a result of enzymatic degradation are lacking.

Herein, we report the development and use of hydrolases to depolymerize model polyester homopolymers and a co-polymer. Two enzymes were investigated for their selectivity in the hydrolysis of small molecules and the depolymerization of structurally diverse polyester (i.e., homopolymers and co-polymers). One of these enzymes was engineered from a hydrolase of the cutinase family to improve its thermostability and allow depolymerization reactions at higher temperatures in aqueous buffer media. The other studied hydrolase was a previously reported variant from the leaf-branch compost cutinase (LCC).[24]

Various LC and LC-MS methods were applied to characterize the products and the remaining polymer after the enzymatic hydrolysis. An overview of the steps performed is presented in SI, Fig. S1. As model polyesters, we selected polymers with different physical and chemical properties (Fig. 1): polyester 1 (PES1) (green box) as an aliphatic polymer based on dodecanedioic acid (DDA, 50%, **2**) and ethylene glycol (EG, 50%, **1**); PES2 (orange box) as a co-polymer with four different monomer units randomly distributed, namely, terephthalic acid (TPA, 37%, **3**), isophthalic acid (IPA, 12%, **4**), neopentyl glycol (NP, 48%, **6**), and adipic acid (ADA, 3%, **5**); and PES3 (blue box) as an aromatic polymer based on terephthalic acid (TPA, 50%, **3**) and ethylene glycol (EG, 50%, **1**).

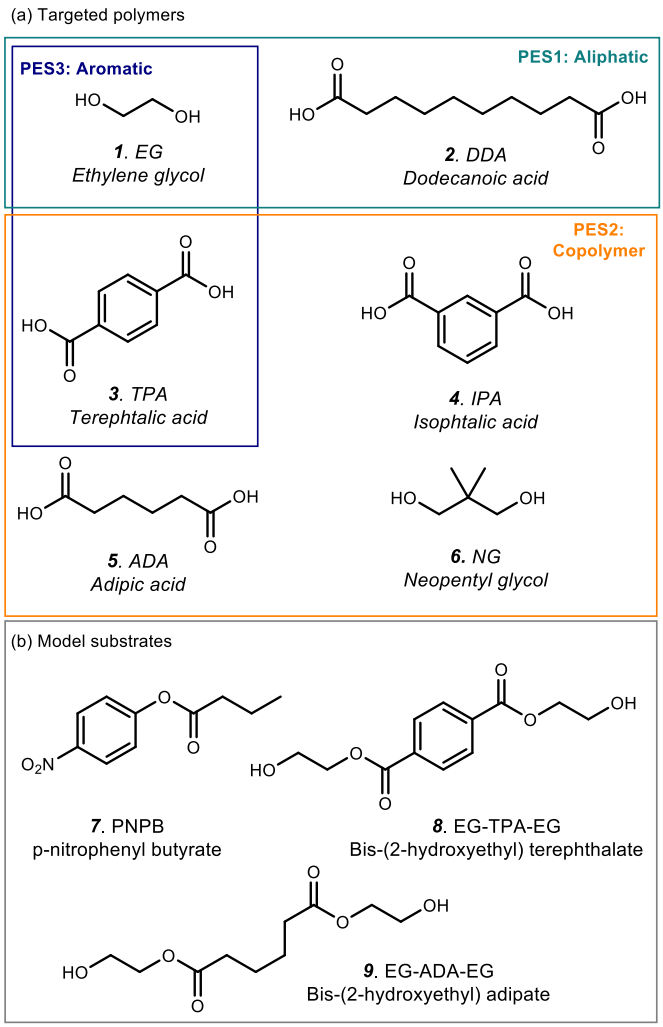

Figure 1. a) Structures of the monomers composing the model polymers enzymatically hydrolyzed and b) model substrates used in this study. The MW of the polymers was determined using SEC against polystyrene standards (see SI, Fig. S3 for details).

Results and discussion

Selection and engineering of thermostable and chemoselective enzymes for the hydrolysis of polyester

We selected a variant of a leaf-branch compost cutinase (LCC^{WCCG}) for its ability to depolymerize PET,[24, 36] and a variant of a cutinase from *Thermobifida cellulosilytica* (Tc_Cut2_R29N_A30V); herein referred as Tc_Cut2NV for its catalytic activity toward PET and polylactic acid (PLA).[42]

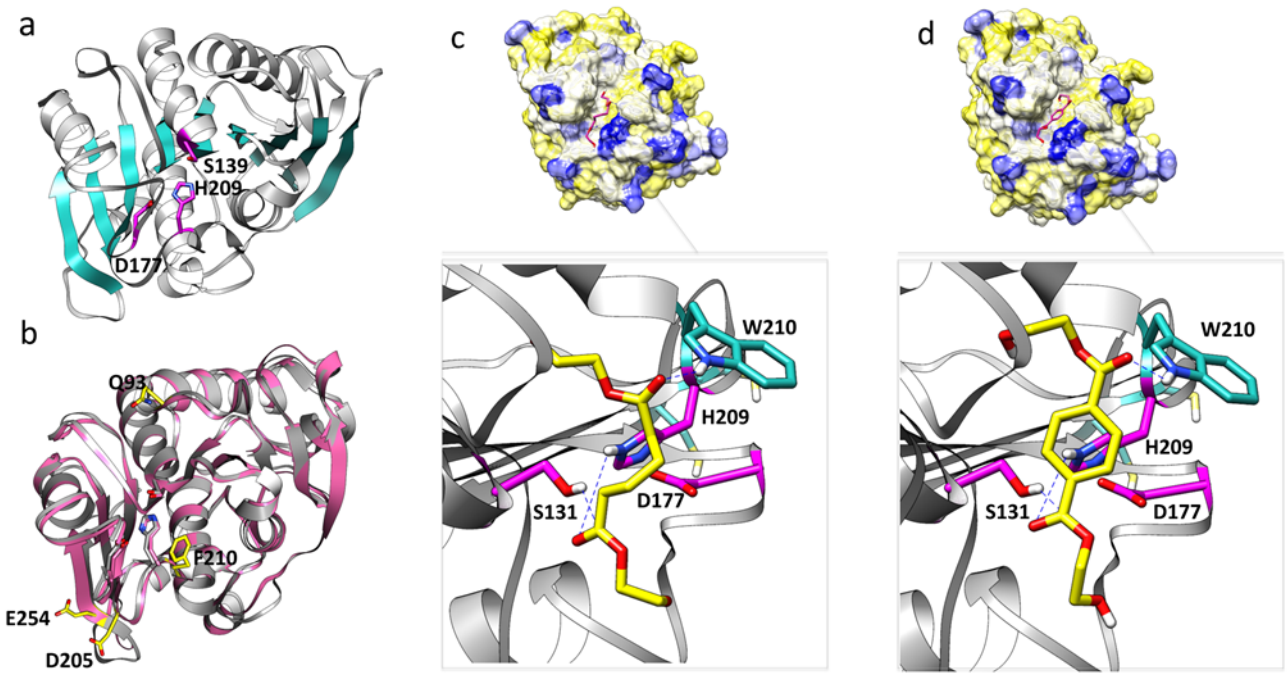

Figure 2. a) Crystal structure of the Tc_Cut2NV (PDB: 5LUK) in which nine antiparallel β-strands (green) are enveloped by ten α-helices displaying a typical α/β-hydrolase fold. The catalytic triad is shown in magenta. B) Crystal structure of wild-type LCC (PDB: 4EB0, magenta) superposed with Tc_Cut2NV. The corresponding residues in Tc_Cut2NV scaffold that generated increased thermostability in the LCC^{WCCG} variant are shown in yellow. c-d) Docking studies with enzyme Tc_Cut2NV^{WCCG} as receptor and using (c) aliphatic oligomer **9** or (d) aromatic oligomer **8** as substrates. The enzyme surface is depicted in blue and yellow to refer to hydrophilic and hydrophobic amino acid residues, respectively. The structures highlight the distance between the catalytic S131 residue and the reactive carbon atom of the oligomers. H209 and the mutated residue W210 are involved in hydrogen bonds with the oxygen atoms of the respective carbonyl moieties. The catalytic triad is shown in magenta, and mutations in light green. Docking was performed using YASARA structure, and Chimera software was used for structural alignment and visualization.

p-Nitrophenyl butyrate (PNPB) was used as model substrate to determine the specific activity of both enzymes at 40 °C. LCC^{WCCG} and Tc_Cut2NV showed 11828 U mg^{-1} and 9904 U mg^{-1} specific activity, respectively.

As the depolymerization reaction rates for the model polyesters increased at higher temperatures, we hypothesized that the reactions could be run at a temperature closer to the glass transition temperature (T_g) of the polymers, therefore increasing polymer chain accessibility (T_g, between 58 and 87 °C, SI Table S1, Fig. S5).[43, 44] We therefore attempted to increase the thermostability of Tc_Cut2NV (>60 °C). Tc_Cut2NV (PDB: 5LUK) has a high structural similarity with the high thermostable variant LCC^{WCCG} (PDB: 4EB0 for wild-type LCC). Both Tc_Cut2NV and wild-type LCC display a typical α/β-hydrolase fold in which nine antiparallel β-strands are enveloped by ten α-helices, five from each side. The enzymes contain an active site serine residue (S131 for Tc_Cut2NV and S138 for LCC) along with the proximal aspartic acid and histidine residues that create a catalytic triad, which is essential for hydrolysis. Figure 2a depicts the X-ray crystal structure of Tc_Cut2NV where the catalytic triad is highlighted (magenta), whereas Figure 2b displays a structural alignment between Tc_Cut2NV (grey) and wild-type LCC (magenta). Due to their high structural similarity, we speculated that introducing similar mutations of the variant LCC^{WCCG} to the scaffold of Tc_Cut2NV might also increase the thermal stability of the latter. Therefore, via 3D-structural alignment, the corresponding residues were identified in the Tc_Cut2NV scaffold and the mutations (Q93G, D205C, F210W and E254C) were introduced to create the Tc_Cut2NV^{WCCG} gene, which was recombinantly expressed in *E. coli* and the enzyme was purified by Ni^{2+}affinity chromatography (SI, Fig. S2) as previously done for Tc_Cut2NV and LCC^{WCCG}.

Thermostability measurements revealed that the mutations in the Tc_Cut2NV^{WCCG} scaffold enhanced the stability of the enzyme, which displayed an impressive melting temperature (T_m) of 91 °C (~27 °C higher than the parental Tc_Cut2NV) (SI, Fig. S4). The new variant also showed a 16% increase in catalytic activity for the hydrolysis of the model substrate PNPB compared with the Tc_Cut2NV (11460 U mg^{-1} and 9904 U mg^{-1} for Tc_Cut2NV^{WCCG} and Tc_Cut2NV, respectively). These results motivated us to conduct long-term thermostability measurements for up to 6 days at 40 °C and 71 °C using purified Tc_Cut2NV^{WCCG}. Results showed that the variant retained its hydrolytic activity at 40 °C even after 6 days (>3000 U mg $^{-1}$) for the model substrate PNPB. The enzyme showed a similar specific activity at 71 °C and at 40 °C (>3000 U mg^{-1}) although the activity at 71 °C decreased 1.6-fold and 6-fold after 3 and 6 days, respectively (Table 1).

Next, we tested whether the introduced mutations improved the tolerance of the enzyme against organic solvents. We chose hexafluoro-2-propanol (HFIP) and tetrahydrofuran (THF) because these solvents can solubilize polyesters, thereby making possible to increase the accessibility of their chains.

Unfortunately, the catalytic activity of Tc_Cut2NV^{WCCG} decreased 30-fold or 40-fold at the tested concentration of added HFIP (10–90% v v^{-1}) (SI, Fig. S6) or THF (50%). This outcome indicated that none of these solvents could be used in the enzymatic depolymerization reactions. Therefore, we decided to conduct all reactions in aqueous buffers devoid of organic cosolvents.

Activity test with model oligomers and structural insights on catalytic activity and selectivity

Next, we assessed whether the enzymes could accept both aliphatic and aromatic oligomers combining wet-lab experiments and computational docking simulations. We used bis-(2-hydroxyethyl) terephthalate (**8**) (EG-TPA-EG) and bis-(2-hydroxyethyl) adipate (**9**) (EG-ADA-EG) (NMR data in SI, Fig. S7) as model substrates because these are structurally similar to the targeted polyester polymers and therefore offer a simplified testbed for our studies.[45-47] Molecular docking simulations using either **8** or **9** as substrates revealed that both Tc_Cut2NV^{WCCG} and LCC^{WCCG} are receptors. Moreover, in the computational models showing the substrate in a productive binding pose, the catalytically active serine (S131 for Tc_Cut2NV^{WCCG} or S165 for LCC^{WCCG}) was found to be in close proximity to the reactive carbon of the substrate carbonyl group (<3 Å) (Fig. 2c and SI, Fig. S8).

Table 1. Long-term thermostability measurements with Tc_Cut2NV^{WCCG} or LCC^{WCCG} with model substrate **7**.

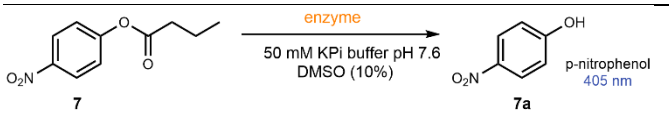

7 **7a**

entry	enzyme	Time (days)	Activity[a] (U mg^{-1})
1	Tc_Cut2NV^{WCCG}	0	4913
2	Tc_Cut2NV^{WCCG}	3	3003
3	Tc_Cut2NV^{WCCG}	6	807
4	LCC^{WCCG}	0	6735
5	LCC^{WCCG}	3	5345
6	LCC^{WCCG}	6	660

[a] Activity was measured by monitoring the increase of the absorbance of **7a** at λ of 405 nm for 1 min using the extinction coefficient (ε 405 nm = 9.36 mL μmol^{-1} cm^{-1}). Reactions were performed with **7** (4 mM) at 71 °C in 50 mM KPi pH 7.6 with the pure enzymes. Measurements were carried out using a spectrophotometer equipped with temperature control. In all measurements, the enzymes were incubated at the desired temperature prior to the assay.

The molecular docking poses in the productive binding modes show the influence of the catalytic histine residue (H209 for Tc_Cut2NV^{WCCG} and H242 for LCC^{WCCG}) in the protonation of the oxygen atom of the carbonyl involved in the hydrolysis reaction. Notably, the introduced tryptophan mutation (F210W for Tc_Cut2NV^{WCCG} or F243W for LCC^{WCCG}) must have had an effect on the positioning of the oligomer substrates in the active site through the possible formation of a hydrogen bond between the NH moiety of the tryptophan residue and the oxygen atom of the second carbonyl (i.e., not involved in the hydrolysis) of the substrate (See Fig. 2).

As predicted by the docking studies, both Tc_Cut2NV^{WCCG} or LCC^{WCCG} could hydrolyze the test oligomers. After 1 or 24 h, we detected the formation by LC-MS of monomer **3** or **5** as the products of the depolymerization of oligomers **8** or **9**, respectively. Within the investigated time-frame (up to 24 h) for the depolymerization of **8** or **9**, LCC^{WCCG} produced a greater amount of the monomer **3** or **5** (near 100% hydrolysis) compared with Tc_Cut2NV^{WCCG} (SI, Fig. S13; around 80% of hydrolysis). Notably, using Tc_Cut2NV^{WCCG}, we detected the formation of partially hydrolyzed intermediates thus maintaining one of the two ester moieties (compound **8a** and **9a** of SI Fig. S13). In contrast, both intermediates were consumed by LCC^{WCCG} after 30 min of reaction. These observations indicate a different reactivity between Tc_Cut2NV^{WCCG} and LCC^{WCCG}, with the latter enzyme being more active. Moreover, the hydrolysis of the aliphatic oligomer **9** catalyzed by LCC^{WCCG} was significantly quicker with respect to the aromatic oligomer **8** within the initial 100 min of the reaction.

Analysis of the depolymerization of homopolyester PES1 and PES3 by RPLC-UV-MS and SEC-UV/RI

After elucidating the different reactivity of Tc_Cut2NV^{WCCG} and LCC^{WCCG} for the hydrolysis of model small molecules and oligomers, we applied the enzymes to the depolymerization of polyesters polymers.

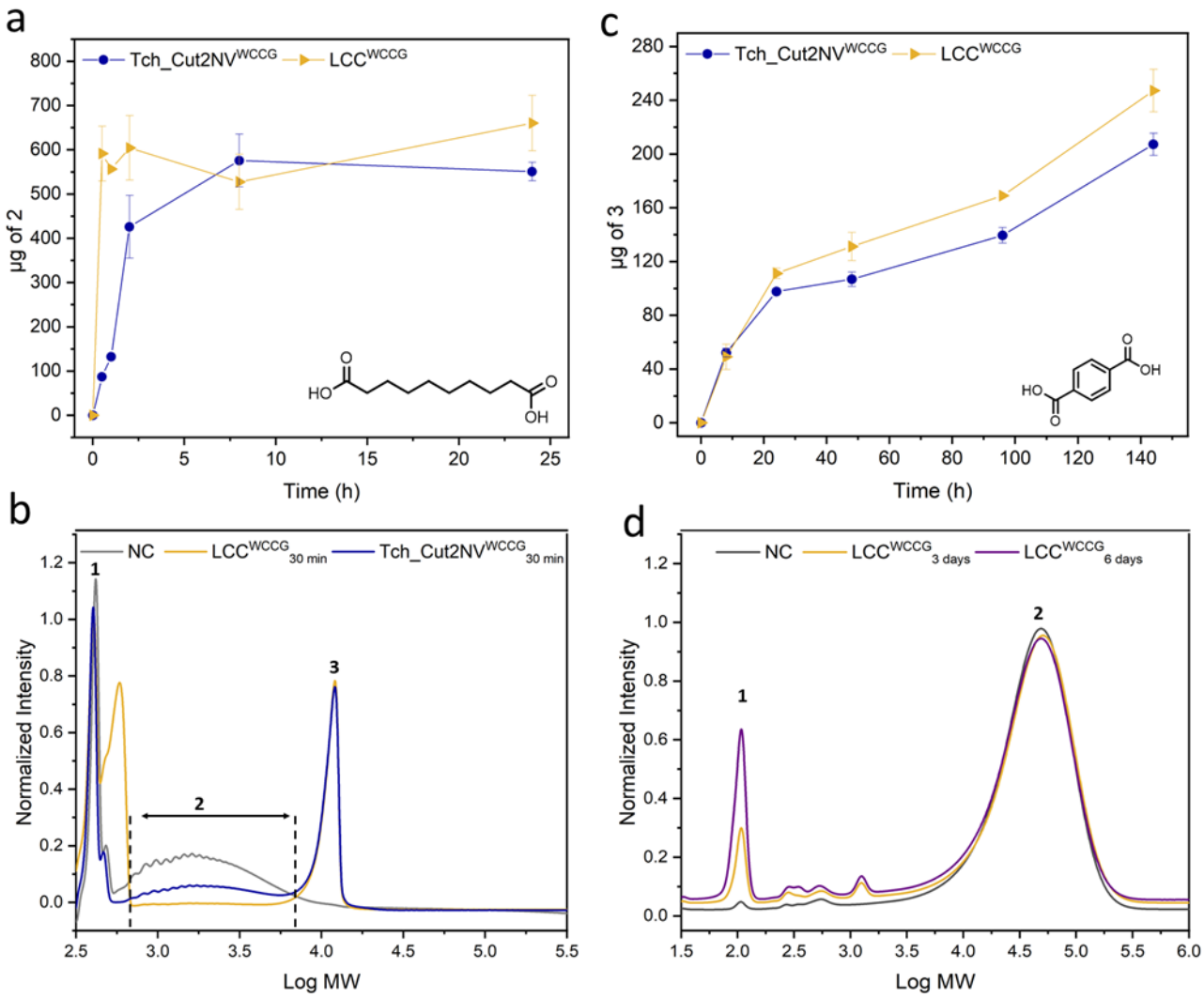

Figure 3. Enzymatic hydrolysis of model polymers PES1 and PES3 catalyzed by Tc_Cut2NV^{WCCG} or LCC^{WCCG}. Reactions were performed with 1 mg PES1 and 1 mg PES3, 1 µM of enzymes at 71 °C in 50 mM KPi. (a) Production of the aliphatic monomer DDA in the depolymerization of PES1; data based on RPLC-MS using the calibration curve from SI, **Fig. S10**. (b) Size exclusion chromatography (SEC) profile of the PES1 samples (polystyrene equivalents) using LCC^{WCCG}, after 30 min (yellow trace) and using Tc_Cut2NV^{WCCG} after 30 min (blue trace); PES1 displayed degradation compared with the negative control without enzymes (grey trace) and complete depolymerization was detected within less than 24 h; 1 indicates the elution area of salts and low molecular weight components, 2 indicates the polymer elution area, and 3 indicates the peak of the enzyme used for the depolymerization; the increase of low molecular weight species 1 with no change in molecular weight distribution was observed as a result of polymer degradation. (c) Production of the aromatic monomer TPA in the depolymerization of PES3; data based on RPLC-UV using calibration curve from SI, **Fig. S11**. (d) SEC profile of PES3 solution in HFIP with LCC^{WCCG} over 6 days; 1 indicates the elution area of salts and low molecular weight components, whereas 2 indicates the polymer elution area. The increase of low molecular weight species 1 with no change in molecular weight distribution was observed due to polymer degradation. For both b) and d) the intensities are normalized to the highest peak to facilitate the comparison. Detailed chromatograms obtained in the PES3 SEC-UV analysis are shown in SI, **Fig. S19**.

The enzymes developed were used to analyze an aliphatic, PES1 (DDA-EG, **2**-**1**), and a aromatic, PES3 (TPA-EG, **3**-**1**), homo-polyester synthetic model (Fig. 1). The polymer samples used in this study were solid materials in different forms such as powder, granules, or blocks. Different strategies to increase the surface area were applied and are described in the supporting information Fig. S9 and S16.

Two methods were used to characterize the hydrolysis products: RPLC-UV-MS to monitor the release of acid monomers in the aqueous reaction mixture (**3**, for PES3, and **2** for PES1) and SEC-UV/RI to analyze the remaining polymer material after centrifugation, sample evaporation, and re-dissolution in HFIP. Details of the RPLC and SEC analysis are presented in SI and Fig. S17-22. SEC-MS was not performed on these polymers as they were not soluble in THF.

Figure 3b illustrates the molecular weight distribution (relative to polystyrene standards) as Log MW plots obtained for the depolymerization reactions of PES1 by LCC^{WCCG} and Tc_Cut2NV^{WCCG} after different reaction times. Negative control experiments (i.e., devoid of enzyme, black trace) were also performed. We observed complete depolymerization of PES1 with LCC^{WCCG} after 30 min (yellow trace) as the polymer distribution area disappeared. In the case of Tc_Cut2NV^{WCCG} (blue trace), the PES1 polymer peak decreased in 30 min and the complete depolymerization was observed within less than 24 h. The process went hand in hand with the progressive

formation of **2** as observed by RPLC-MS and the visual observation of the complete degradation of PES1 in the reaction mixture.

In the case of PES3, limited amount of **3** was released in the first 24 h of reaction time; therefore, the reaction time was extended up to 6 days (results are presented in Fig. 3c). A slightly higher amount of monomers were released when LCC^{WCCG} was used instead of Tc_Cut2NV^{WCCG}. Extending the reaction time from 1 to 6 days doubled the amount of produced TPA (110 µg and 90 µg after 1 day to 235 µg and 213 µg after 6 days using LCC^{WCCG} and TC_Cut2NV^{WCCG} respectively). However, a significant portion of polymer could still be observed in solution and was measured by SEC-UV (Fig. 3d). This analysis revealed a decrease of about 44% and 25% of the polymer peak area after 6 days for LCC^{WCCG} and TC_Cut2NV^{WCCG,} respectively (SI, Fig. S19). Despite the significant release of monomer recorded by RPLC-UV-MS and the formation of small MW species observed in SEC-UV over the reaction time, we noticed negligible changes in the molecular weight distribution (M_n and Mw) of the polymer peak. Therefore, we conclude that for both homopolymers, the hydrolysis occurred primarily at the end groups of the polymers.

Molecular characterization of PES2 LCC hydrolysis by SEC-MS

Finally, we applied the enzymatic depolymerization reactions discussed above to the aromatic-aliphatic co-polyester PES2, which is a randomly distributed co-polymer made of 49% aromatic acid monomer (TPA+IPA, **3**+**4**), 3% aliphatic acid monomer (ADA, **5**) and one alcohol (NG, **6**) (further details in Fig. 1 and Table S1).

Our analysis focused on the depolymerization of co-polymer PES2 for 6 days with 1 µM LCC^{WCCG} or Tc_Cut2NV^{WCCG} compared to the negative control.[48] RPLC-UV and SEC-UV results from the hydrolysis of the polymer using LCC^{WCCG} and Tc_Cut2NV^{WCCG} can be found in Fig. S20 and 22. RPLC-UV results revealed a slow hydrolytic behavior of PES2, similar to that of PES3. However, unlike for the homopolymer PES3, SEC-UV analysis of the unsoluble polymer revealed that PES2_LCC sample (i.e., depolymerization of PES2 by LCC^{WCCG}) presented a significant reduction in molecular weight (Mn from 9748 to 6223 and Mw from 16809 to 11824). Limited MW reduction was observed for the PES2 sample treated with Tc_Cut2NV^{WCCG} (Mn from 9748 to 9480 and Mw from 16809 to 16170).

To identify the monomer composition of the species detected by SEC-UV and elucidate possible chemical composition changes, the degradation products—insoluble in the reaction media—were solubilized in THF and analyzed by SEC-UV/ESI-MS.[49] While UV detection provided information on the entire polymer molecular weight distribution, as shown in Figure 4a, MS hyphenation enabled the identification of the chemical composition of a wide range of oligomers (up to 5300 Da). Due to health hazards and ESI compatibility, we adopted THF as the solvent for the SEC-MS analysis. Similar profiles were observed between SEC in THF and HFIP for this polymer.

A systematic data analysis approach was applied to the MS spectra recorded during SEC separation. For clarity, only a fraction of the mass spectra is depicted in Figure 4a (signals sum from 8 to 9 min of SEC elution) and only the results for the samples treated with LCC^{WCCG} and the negative control are reported. Details of the assignments as well as data for PES2 treated with Tc_Cut2NV^{WCCG} are provided in the SI (Fig. S24 and S25; Table S3 to S5). Results with Tc_Cut2NV are not discussed as we observed a lower level of hydrolysis with this enzyme.

Our data analysis revealed two important changes in PES2 upon hydrolysis by LCC^{WCCG}: (i) changes in polymer end groups and (ii) changes in monomer composition.

(i) Polyesters exhibit different end-group compositions depending on how they have been synthesized.[49, 50] The mass spectra obtained from the original polymer sample PES2_NC (control experiment for PES2 with no enzyme in the media (Fig. 4b,c) features three different end-group types—i.e., di-acid, mono-acid, di-alcohol—as well as cyclic chains (lacking end-group contribution in their mass). The cyclic, di- and mono-acid terminated chains are the most abundant signals in the spectra of the starting material making 85% of the sum of the monoisotopic peaks (51% being cyclics, 34% mono-acid, 14% di-acid and 1% di-alcohol terminated). This results only partially agrees with NMR data where acid end-groups accounted for ca. 14 mol% over the MW range (Tab. S2). Because of known ionization yields differences of end groups in ESI-MS, it not possible to comment on the relative abundance of oligomers as a function of their chain-end in the same sample. However, it is possible to assess differences in their relative contributions between samples. In particular, the MS signature of the degraded PES2_LCC sample (Fig. 4d) differs significantly from the MS profile of the original polymer. Here signals assigned to di-alcohol-terminated chains are predominant, with 88% of the sum of the monoisotopic peak intensities. The secondary most abundant signals were assigned to cyclic oligomers, while peaks assigned to mono- and di-acid terminated chains were in the minority, with intensities of 10% and 2% maximum, respectively. Experiments by changing the ionization additive from sodium to ammonium revealed similar end-group changes.

Additionally, after hydrolysis, almost all the cyclic polymers disappeared, suggesting that they were hydrolyzed into the linear polymer.

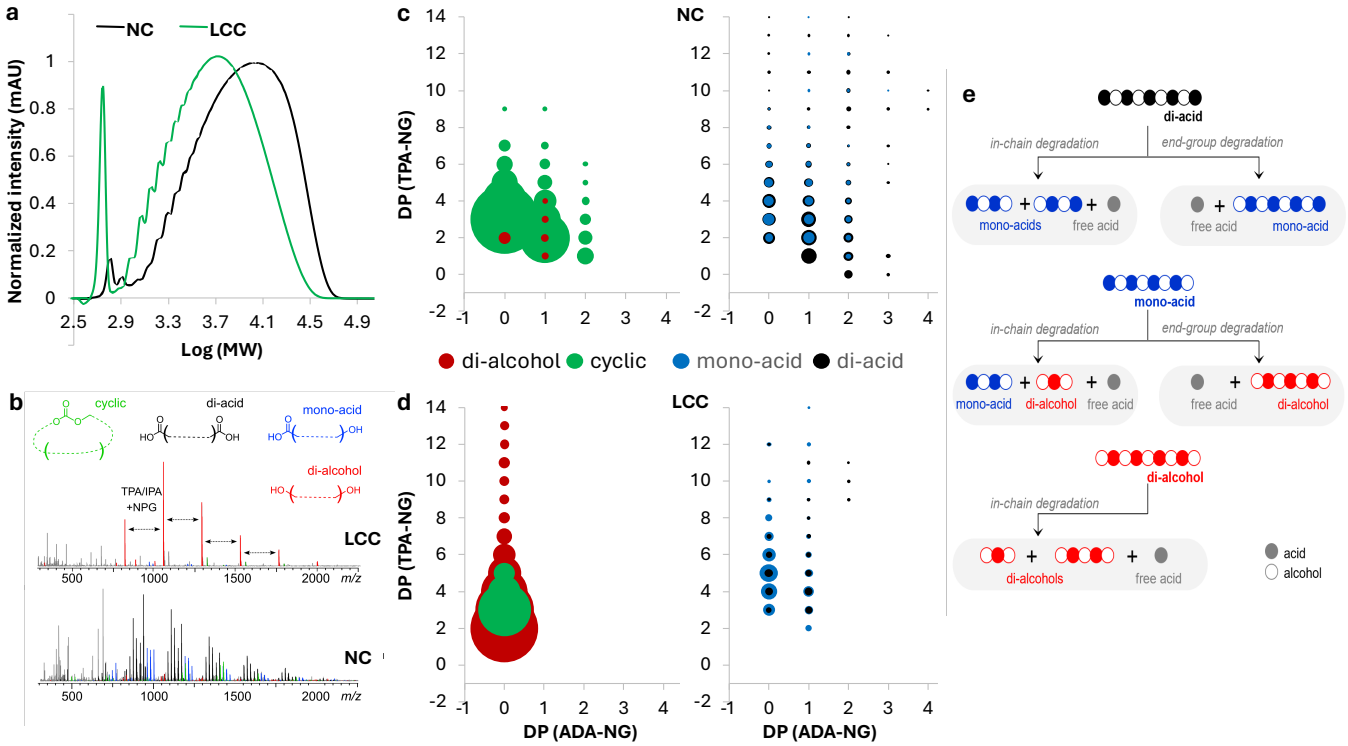

Figure 4. a): Molecular weight distributions of PES2_control (NC, black trace) and after hydrolysis using LCC^{WCCG} (LCC, green). The log MW is acquired via SEC-UV and relative to polystyrene standards (SI, **Fig. S23**). b) From top to bottom, respectively, mass spectra averaged over 1 min of SEC elution (8 to 9 min) for PES2 depolymerized with LCC^{WCCG} (LCC) and its control experiment (NC). MS peaks are assigned to a given end-group pair by color: mono-acid (blue), di-acid (black), di-alcohol (red) and cyclic (green). The grey signals are assigned to background noise and sodium iodide (NaI) clusters. All peaks above 0.2% intensity were processed in a semi-automated fashion using MSPolyCalc[51] and based on the known polymer compositions. The data processing resulted in molecular formula assignments within a mass tolerance of 5 ppm and with good isotopic pattern match (within 95% similarity for isotopic zones up to A+3). All species were detected in positive ion mode as $[M+zNa]^{z+}$ sodium adducts with charge states (z) ranging from 1 to 3. c,d) Bubble chart reporting the assigned molecular formula from the SEC-MS analysis as a function of the number of polymer units (degree of polymerization, DP) of aromatic-based monomers (TPA/IPA-NPG; **3**,**4**-**5**) versus aliphatic monomers (ADA-NPG; **2**-**5**) for (c) PES2_LCC and (d) PES2_control. The dimension of the bubbles is scaled with the maximum intensity in the MS plot (alternative representation in SI, **Fig. S24** and **25,** data available in SI Table S3-5). e) Schematic representation of polymer chain degradation as a function of types of end groups.

Figure 4e illustrates the proposed mechanism of degradation that results in the release of di-acids from variable polyester chains as a function of their end-group type. As illustrated, the hydrolysis process gradually yields to the release of acid terminated monomers and the fully alcohol-terminated polymer chains, regardless of the localization of the cleavages (i.e., at the end of, or within the chain).

(ii) The composition of the oligomers in terms of aromatic and aliphatic content was retrieved by mass analysis. Figure 4c-d summarizes the degree of polymerization (DP, here measured up to 14) of aromatic monomers as a function of the DP of aliphatic monomers observed in the SEC-MS experiments.

In PES2_NC sample, several congeners exist with variable DP of aliphatic acid (**2**) ranging from 0 to 4, with the aromatic DP being between 1 and 14 (**3** and **4** cannot be distinguished from each other because they are isobaric). This situation changes significantly when analyzing PES2_LCC sample. In this case, the species detected in the same molecular weight range are deprived of aliphatic acid (**2**). In particular, the assigned mono-acid terminated chains of PES2_LCC sample carry 0 to 1 aliphatic monomer and the intensities of the signals are below 10%. In contrast, the di-acid terminated chains were detected with a maximum of two aliphatic units and an intensity of 2% maximum.

Based on these observations, we conclude that the reduction in molecular weight observed by enzymatic hydrolysis is likely to occur via in-chain hydrolysis and at the sites of the aliphatic monomers rather than at the polymer end group. These results agree with the different hydrolysis rates that the enzymes exhibited toward aliphatic or aromatic homopolymers. It should be noted that the list of assignments is representative of the lower mass portion of the sample; however, we expect the same trend to apply to higher molecular weight species.

Experimental

Methods

Enzymes expression and purification

For heterologous expression, *E. coli* BL21(DE3) competent cells harboring the corresponding pET-21a(+) plasmid for Tc_Cut2NV, or

Tc_Cut2NV^{WCCG}, or LCC^{WCCG} were grown at 37 °C, overnight in LB medium containing 100 µg mL^{-1} ampicillin (overnight cultures). The next day, cultures of 800 mL were inoculated with 15 mL of the overnight culture (dilution 1:50). The expression of the enzymes was induced by the addition of 0.1 mM (final concentration) isopropyl β-D-thiogalactoside (IPTG) when the absorbance at 600 nm was at 0.7–1. Induction was performed at 20 °C, overnight. After this time, a small sample of each culture was used to determine the expression with SDS-PAGE. *E. coli* BL21(DE3) cells containing the biocatalyst were harvested by centrifugation at 4500 × g for 20 min at 4 °C, resuspended in lysis buffer (50 mM sodium phosphate buffer, 10 mM imidazole, 10 mM NaCl, pH 8) and sonicated for 10 min (total sonication time: 10 min, amplitude: 45%, Pulse ON: 10 sec, Pulse OFF: 15 sec). The lysates were centrifuged at 20000 rpm for 60 min at 4 °C. The supernatant was collected, filtered through a 0.45 µm filter, and protein purification was performed by Ni-NTA affinity chromatography using pre-packed Ni-NTA HisTrap FF columns (GE Healthcare) according to the manufacturer´s instructions. Equilibration of the column (5 mL) was performed with 10 CV lysis buffer (50 mM KH_2PO_4, 300 mM NaCl, 10 mM imidazole, pH 8.0). After that, the filtrated supernatants were loaded into the columns. Two washing steps were carried out with 10 CV lysis and 10 CV wash buffer (50 mM sodium phosphate buffer, 25 mM imidazole, 300 mM NaCl, pH 8). The enzymes were finally eluted (10 x 1 mL) with elution buffer (50 mM sodium phosphate buffer, 200 mM imidazole, 300 mM NaCl, pH 8). The process of purification was analyzed by SDS-PAGE. The elution fractions containing the enzyme were combined and concentrated through a 30 kDa filter. Buffer exchange was performed using PD-10 columns.

Activity test of purified enzymes for the model substrates

Esterase activity was measured at different temperatures using p-nitrophenyl butyrate (PNPB) as a substrate. Reactions of 1.11 mL contained 1 mL of 50 mM phosphate buffer at pH 7, 100 µL of enzyme (after dilution), and 10 µL of PNPB (4 mM). The increase of the absorbance at 405 nm was monitored using a spectrophotometer for 1 min. A blank was measured with 100 µL buffer instead of enzyme. The increase of the absorbance indicated an increase of p-nitrophenol (ε_{405nm} = 9.36 mL µmol^{-1} cm^{-1}) due to hydrolysis of the PNPB. The activity was calculated in units per mL, where 1 unit is the amount of enzyme required to hydrolyze 1 µmol of substrate per minute under the assay conditions. In cases where the enzyme was used in purified form, the activity was also expressed as U mg^{-1} by dividing the value previously obtained (U mL^{-1}) by the enzyme concentration (mg mL^{-1}). For the calculation of the specific activity, the equation 1 was used where f refers to the dilution factor and k to the obtained slope. For the long-term stability of the enzymes, prior to the measurements, the enzymes were incubated various times in the reaction buffer at different temperatures.

Equation 1. The equation used to calculate the specific activity of the enzymes. k refers to the obtained slope (min^{-1}), A to the volumetric activity (U mL^{-1}), V_{total} to the total volume (1.11 mL), f to the dilution factor of the enzyme sample, V_{sample} to the enzyme sample volume (0.1 mL), ε to the molar extinction coefficient (8.80 mL µmol^{-1} cm^{-1}), and d to cuvette length (1 cm).

$$A = \frac{k \cdot V_{total} \cdot f}{V_{sample} \cdot \varepsilon \cdot d}$$

Determination of the T_m of the enzymes

The T_m of the purified enzymes (melting temperature Tm, defined as the temperature at which 50% of the enzyme unfolds) was determined in 50 mM KPi pH 7.6 buffer by differential scanning fluorometry using a Biorad-7500 QPCR machine. Each reaction mixture (20 µL) contained SYPRO orange (5 µL, stock 20x in qH_2O), 2 µg of the enzyme, and the buffer. Fluorescence data were collected as a continuous standard melt curve from 20–90 °C (1% increment, held 1 min at 20 °C and 1 min at 90 °C), using ROX for the reporter and none for a quencher. Moreover, none was selected as a passive reference. Three reaction replicates were prepared for each enzyme used, as well as a negative control without enzyme.

Computational studies

The crystal structures of Tc_Cut2NV (PDB: 5LUK) and LCC (PDB: 4EB0) were used as initial templates. A structural alignment of these templates was performed using the matchmaker tool incorporated in UCSF Chimera. Thus, the corresponding residues that conferred increased thermostability for LCC were identified in the structure of Tc_Cut2NV. These residues were in silico modified (Q93G, D205C, F210W, E254C) using YASARA structure[52] with AMBER 03 as force field.[53] After the introduction of a mutation or modification, the energy of the system was minimized following a three-step protocol that enables the adjustment of the model structure without creating any possible unwanted deformation. In step one, only the atoms constituting the mutated amino acid residue were subjected to energy minimization. In step two, the process for energy minimization was repeated by including all the atoms of the amino acid residues that were located within 6 Å distance from the mutated residue. In step three, the energy of the overall structure was minimized. The molecular dockings were performed using Autodock Vina as tool implemented in YASARA. The simulation box was placed around the active site residues S131, H209, and D177 for Tc_Cut2NV and S165, H242, and D210 for LCC^{WCCG} at 10 Å. A total of 25 VINA docking runs of each ligand to the receptor were run. After clustering the 25 runs, all distinct complex conformations were sorted by binding energy (more positive energies indicate stronger binding). The resulting models were inspected visually.

Synthesis of polymer model substrates

PES 1

A reactor vessel fitted with a thermometer, a stirrer, and a distillation device for the removal of water formed during the synthesis was filled with butylstannoic acid (0.1 wt%) as catalyst, 50 mol% of EG, and 50 mol% of dodecanedioic acid. The vessel was gradually heated up to 230 °C under nitrogen flow with a heating mantle while distilling off the reaction water until the mixture was clear and water was no longer coming off. The mixture was cooled to 220 °C and vacuum was applied until the polyester reached a hydroxyl value below 10 mg KOH/g (titrimetrically measured in tetrahydrofuran according to ISO 4629-2:2016). The viscous material was cooled to 180 °C and discharged on aluminum foil to solidify.

PES 2

A reactor vessel fitted with a thermometer, a stirrer, and a distillation device for the removal of water formed during the synthesis was filled with butylstannoic acid (0.1 wt%) as a catalyst and 48 mol% of neopentyl glycol (based on total amount of monomers). The vessel was heated up to 150 °C under nitrogen flow with a heating mantle until the mixture was molten. Terephthalic acid (37 mol%) and isophthalic acid (6 mol%) were then added and the temperature was gradually increased to 260 °C while distilling off the reaction water until the mixture was clear and no water was coming off. The mixture was cooled to 180 °C and isophthalic acid (6 mol%) and adipic acid (3 mol%) were added after which the temperature was gradually increased to 250 °C while distilling off water. When water was no longer distilling off, a vacuum was applied at 250 °C until the polyester reached a hydroxyl value below 10 mg KOH/g (titrimetrically measured in tetrahydrofuran according to ISO 4629-2:2016). The viscous material was cooled to 180 °C and discharged on aluminum foil to solidify.

PES 3

This is recycled PET from Cumapol being the Ecoclear E00 100 grade.

PES3 thin film layer or nanoparticle preparation

The PES3 used to produce a thin film layer was obtained as hard blocks; 0.1 gram of the PES3 was fully dissolved in 0.5 mL of HFIP at room temperature by shaking the vials from time to time to avoid using a magnetic bar in this solvent. Next, the solution was spread over a glass plate and dried in the fume hood to form a very thin layer of plastic. The plate was kept in the fume hood overnight until the thin layer dried completely, and was then collected. In another batch, after dissolution, the solution was added drop by drop to 10 mL of distilled water under vigorous stirring. The solution was kept stirring overnight. The precipitated particles were then removed by decantation and dried on filtration paper at room temperature.

Synthesis of di-β-hydroxyethyladipate

A reactor vessel fitted with a thermometer, a stirrer, and a distillation device for the removal of water formed during the synthesis was filled with *p*-toluenesulfonic acid (0.1 wt%) as a catalyst, adipic acid, and a ten-fold mole excess of ethyleneglycol. The vessel was heated to 150 °C under nitrogen flow with a heating mantle for 5 h while distilling off any reaction water formed. The mixture was cooled to room temperature and ethylacetate was added together with water to remove the catalyst and ethyleneglycol by extraction. After a first separation of the water layer, the ethylacetate was washed several times with water and the (wet) ethylacetate was removed in a rotary evaporator to leave the desired product.

Determination of the MW of the polymers by SEC

The MW of the polymers was calculated using a PFG Linear XL column by determining the retention time of PMMA (1.5 mg mL^{-1} HFIP) of known MW standards polymers. The retention times of the PMMAs were plotted against their log size and the resulting trendline was used as a calibration curve to calculate the MW of the polymers (PES1, PES2, and PES3). The MW of PES1 was calculated based on the retention time of the RI detector. For all other polymers, the MW was calculated based on the retention times observed by the UV-detector (220 nm).

Number average molecular weight, Mn, was calculated as:

$$Mn = \frac{\sum NiMi}{\sum Ni}$$

Weight average molecular weight, Mw, was calculated as:

$$Mw = \frac{\sum NiMi^2}{\sum NiMi}$$

Mi is the molecular weight of a chain calculated as polystyrene equivalent and Ni is the number of chains of that molecular weight obtained from the intensity (UV or RI).

Polydispersity index was calculated as:

$$PDI = \frac{Mw}{Mn}$$

RPLC analysis of the depolymerization reactions for polyesters to detect the soluble monomers TPA and DDA

Enzymatic depolymerization reactions of 1 mL containing 1 mg mL^{-1} of PES1, PES2, or PES3 and using either TcCut2NV^{WCCG} or LCC^{WCCG} (1 µM) were analyzed. In addition, a negative control was prepared for each polymer without any enzyme present. The Eppendorf tubes (reactions and negative control) were shaken in a thermomixer at 800 rpm, at 71 °C for different amounts of time. After the reaction times, an aliquot of 150 µL was taken from the reaction mixture and mixed with 150 µL of acetonitrile and 4 µL of 6 M HCl. The samples were filtered through a 0.45 µM filter and analyzed by RP-HPLC. The peak for the soluble aromatic monomer was assigned by comparison to commercial chemical standard TPA. The peak for the soluble aliphatic monomer was assigned by using LC-ESI-MS detector comparison to commercial chemical standard DDA. The targeted m/z for DDA is 229 (with a value M-H^+).

SEC-UV analysis of depolymerization reactions for polyesters

The enzymatic depolymerization reactions were performed with 1 µM of enzyme (TcCut2NV^{WCCG} or LCC^{WCCG}). In all cases, the reactions of 1 mL were performed with 1 mg mL^{-1} of polymer in 50 mM KPi buffer pH 7.6 (insoluble polymer present). After the desired reaction time, the aqueous phase was removed under reduced pressure using a SpeedVac (60 °C, 4 h, V-AQ mode). Next, 1 mL of HFIP was added to the reaction tube. The volume of HFIP added remained the same as the volume of the buffer when the reaction was started in order to keep the concentration of the starting polymer the same. The samples were incubated for 30 min, 35 °C, 700 rpm in a thermomixer with shaking. After that time. the organic phase was filtrated through a 0.45 µM filter and analyzed by SEC-UV.

SEC-MS analysis of depolymerization reactions for polyesters

After the reactions finished, the aqueous phase was removed under reduced pressure using a SpeedVac (60 °C, 4 h, V-AQ mode). Next,

unstabilized THF with 0.1% FA was added to the reaction tube. The samples were incubated for 30 min, 35 °C, 700 rpm in a thermomixer with shaking. Finally, the organic phase was filtrated through a 0.45 µM filter and analyzed by SEC-MS.

Analytical methods

RPLC-UV

Reaction mixtures were analyzed using Agilent Zorbax C18 RRHD, 50 mm x 2.1 mm x 1.8 µm, gradient mode, mobile phase (A) H_2O containing 0.05% acetic acid, (B) acetonitrile containing 0.05% acetic acid (0% B, 2 min; 2% B, 2 min; 100% B, 10 min; 100% B, 14 min; 2% B, 15 min; 2% B, 20 min). Flow rate 0.2 mL min^{-1}, oven temp. 60 °C. Samples soluble in buffer/ACN (1:1). The UV spectrum was recorded at 245 nm (λ_{max} = 245 nm, Injection volume 5 µL).

RPLC-ESI-MS

The samples were next analyzed by LC-electrospray (ESI)-MS (Thermo Finnigan LTQ system) (Thermo Fisher, Waltham, USA). The RPLC separation was conducted using the same method as RPLC-UV analysis. Samples were analyzed under ESI positive and negative mode (ESI+/ ESI-) with a source voltage of 3.0 kV, heater temperature of 50 °C, and a capillary temperature of 275 °C. Nitrogen was used as the drying gas. MS data were acquired in the m/z 50–1000 range.

SEC-UV

The samples were analyzed by size exclusion chromatography (SEC) using two columns depending on the estimated MW average, Mn, Mw, and PDI for each polymer. For PES2 and PES1, Acquity APC XT 25 A, 4.6 mm ID, 150 mm long, 1.7 µm particles, from Waters was used with isocratic separation mode. The eluent was HFIP at 0.150 mL min^{-1} flow rate, column oven thermostated at 30 °C, 40 min, detector B 220 nm. For PES3, PSS Linear XL 8 X 300 mm, 7 µm particles, two columns were used with isocratic separation. The eluent was HFIP at 0.600 mL min^{-1} flow rate, column oven thermostated at 30 °C, 60 min, detector B 220 nm. Results and calibration curves are presented in the SI (Table S1,2, Fig. S3 and S23).

SEC-UV-MS

The system comprised a binary solvent manager, sample manager equipped with a 5 µL sample loop, column manager and PDA detector equipped with an analytical flow cell (V_{det} = 500 nL). For SEC-HRMS experiments, a similar Waters Acquity system was connected to a Waters Synapt G2 high-resolution mass spectrometer.

The SEC–UV-Vis/HRMS method was performed using one Acquity APC XT 45 A, 4.6 mm ID, 75 mm long, 1.7 µm particles and one Acquity APC XT 125 A, 4.6 mm ID, 75 mm long, 1.7 µm particles; the columns were in series. 10 µL of solute was injected onto the SEC column set operated at a flow of 0.18 mL min^{-1} THF containing 0.1% (v/v) formic acid and thermostated at a temperature of 50 °C. Using restriction capillaries, the effluent was split 9:1 to the UV-Vis and HRMS detector, respectively. At the mass spectrometer, a make-up flow based on 90% MeOH and 10% 1 mM NaI run at of 20 µL min^{-1} was infused to create a total flow to the ESI inlet of 40 µL min^{-1}, with a 1:1 ratio of analytical and make-up flow.

The MS method had two measuring ranges combined: m/z range, 50-700 and 700-3000. The scan time was 1 s positive ESI; time-of-flight MS Resolution mode; capillary voltage, 3.0 kV; sampling cone, 100 V; trap collision energy, 20 eV; source temperature, 100 ˚C; desolvation temperature, 250 ˚C; nitrogen desolvation gas flow, 800 L h^{-1}; nebulizer gas flow, 100 L h^{-1}. Mass calibration was performed using a NaI solution.

Data processing was carried out using the web-based application MSPolyCalc (accessible at www.polycalc.org).* Spectra were calibrated post-acquisition via the assignment of sodium iodide clusters $[(NaI)n^{+}\ Na]^{+}$. The monomer units were defined as the acid-alcohol pairs: TPA/IPA+NPG ($C_8O_2H_4C_5O_2H_{10}$) and ADA+NPG ($C_6O_2H_8C_5O_2H_{10}$). Mass analysis was performed using the following parameters: peak picking threshold 0.2% (intensities normalized to highest signal), mass tolerance 10 ppm; isotopic zone comparison - 0.5 < zone < 2.5 Da in most cases; similarity threshold between 80% and 90% depending on the charge state.

The SEC-MS data (Fig. 4, and SI, Fig. S24 and S25 and Table S3) have been deposited to the MassIVE Archive identifier MSV000090842 (ftp://massive.ucsd.edu/MSV000090842/

Conclusions

In this study, we described an in-depth analytical characterization of the process of hydrolysis of polyester polymers catalyzed by a recently described cutinase (LCC^{WCCG}) and a homologue cutinase variant that was created and reported for the first time in this work (Tc_Cut2NV^{WCCG}). Model small molecules, aliphatic and aromatic polyesters as well as an aromatic-aliphatic co-polyester were investigated for their depolymerization with the chosen hydrolases. RPLC-UV-MS analyses allowed us to monitor the water-soluble products released by hydrolysis. SEC-MS analysis allowed us to gain insight into the monomer composition of the species resulting from the enzymatic hydrolysis.

We conclude that the mechanism of the enzymatic hydrolysis catalyzed by LCC^{WCCG} and TC^{WCCG} is similar and that in co-polymer systems the enzymes selectively depolymerize the constituting monomers depending on their chemicophysical characteristics such as in the case illustrated here of aliphatic and aromatic monomers. The results and method proposed herein give insights into the mode of hydrolysis of these hydrolases in polyester co-polymer systems, thereby providing information for the rational engineering of more selective and catalytically active enzymes. Furthermore, these results could be exploited as a starting point for developing analytical workflows in which the selectivity of enzymes is harnessed to characterize the co-polymer distribution in a polymer sequence.

Author Contributions

E.A., V.T., J.D., A.F.G.G. and F.G.M. wrote the manuscript. E.A., V.T. , A.F.G.and J.D. created the figures and schemes. E.A. performed depolymerization reactions; characterization analysis; data interpretation; and contributed to enzymes purification and

thermostability and activity assays. V.T. performed bioinformatic analysis; enzyme evolution, expression and purification; thermostability and activity assays; and all the tasks related to computational studies (homology models, dockings). A.F.G.G designed the separation and mass spectrometry method; and performed and supported data visualization and interpretation. A.F.G.G. and J.D. performed the SEC-MS measurements. J.D. performed the SEC-MS data interpretation and visualization. F.G.M. reviewed the computational structural models of the enzymes. P.B. performed the synthesis of the polymer models and the small model substrates. M.S. and R.P. provided intellectual input, support to supervision, and material and resources during the implementation of the project. A.F.G.G. and F.G.M acquired the funding, and designed and directed the research.

Conflicts of interest

There are no conflicts to declare.

Acknowledgements

This research was funded by Topconsortium voor Kennis en Innovatie (TKI) Chemie, deployment project PPS-programmatoeslag 2019 (CHEMIE.PGT.2020.020). Contribution from Covestro Resins & Functional Materials, and InnoSyn B.V. are acknowledged. We thank Harry Philipsen (DSM Geleen) for the insightful discussions.

Keywords: co-polyesters • selective enzymatic hydrolysis • SEC-MS • hydrolases • biocatalysis.

Notes and references

1. E. F. Izard, The effect of chemical composition on selected physical properties of linear polymers, *J. Polym. Sci.*, 1952, **8**, 503-518.
2. M. Gilbert and F. J. Hybart, Effect of chemical structure on crystallization rates and melting of polymers: Part 1. Aromatic polyesters, *Polymer*, 1972, **13**, 327-332.
3. R. B. Seymour and C. E. Carraher, in *Structure—Property Relationships in Polymers*, eds. R. B. Seymour and C. E. Carraher, Springer US, Boston, MA, 1984, DOI: 10.1007/978-1-4684-4748-4_1, pp. 1-17.
4. B. Klumperman, R. Pfukwa and A. Lederer, in *Macromolecular Engineering: From Precise Synthesis to Macroscopic Materials and Applications, Volume 3: Macromolecular Architectures*, eds. K. Matyjaszewski, Y. Gnanou, N. Hadjichristidis and M. Muthukumar, Wiley-VCH, 2022, DOI: doi.org/10.1002/9783527815562.mme0024, pp. 1-52.
5. E. F. Palermo and A. J. McNeil, Impact of Copolymer Sequence on Solid-State Properties for Random, Gradient and Block Copolymers containing Thiophene and Selenophene, *Macromolecules*, 2012, **45**, 5948-5955.
6. A. J. Trazkovich, M. F. Wendt and L. M. Hall, Effect of copolymer sequence on structure and relaxation times near a nanoparticle surface, *Soft Matter*, 2018, **14**, 5913-5921.
7. C.-L. Lin, W.-C. Chen, C.-S. Liao, Y.-C. Su, C.-F. Huang, S.-W. Kuo and F.-C. Chang, Sequence Distribution and Polydispersity Index Affect the Hydrogen-Bonding Strength of Poly(vinylphenol-co-methyl methacrylate) Copolymers, *Macromolecules*, 2005, **38**, 6435-6444.
8. A. Staubli, E. Mathiowitz and R. Langer, Sequence distribution and its effect on glass transition temperatures of poly(anhydride-co-imides) containing asymmetric monomers, *Macromolecules*, 1991, **24**, 2291-2298.
9. Y. Kametani, F. Tournilhac, M. Sawamoto and M. Ouchi, Unprecedented Sequence Control and Sequence-Driven Properties in a Series of AB-Alternating Copolymers Consisting Solely of Acrylamide Units, *Angew. Chem. Int. Ed.*, 2020, **59**, 5193-5201.
10. D. M. Bigg, Polylactide copolymers: Effect of copolymer ratio and end capping on their properties, *Adv. Polym. Tech.*, 2005, **24**, 69-82.
11. T. N. J. Fouquet, H. Pizzala, M. Rollet, D. Crozet, P. Giusti and L. Charles, Mass Spectrometry-Based Analytical Strategy for Comprehensive Molecular Characterization of Biodegradable Poly(lactic-co-glycolic Acid) Copolymers, *J. Am. Soc. Mass. Spectrom.*, 2020, **31**, 1554-1562.
12. Q. Y. Lee and H. Li, Photocatalytic Degradation of Plastic Waste: A Mini Review, *Micromachines*, 2021, **12**.
13. Y. Lin, T. B. Kouznetsova, C.-C. Chang and S. L. Craig, Enhanced polymer mechanical degradation through mechanochemically unveiled lactonization, *Nat. Commun.*, 2020, **11**, 4987.
14. R. K. Singh, B. Ruj, A. K. Sadhukhan and P. Gupta, Thermal degradation of waste plastics under non-sweeping atmosphere: Part 1: Effect of temperature, product optimization, and degradation mechanism, *J. Environ. Manage.*, 2019, **239**, 395-406.
15. Å. M. Ronkvist, W. Xie, W. Lu and R. A. Gross, Cutinase-Catalyzed Hydrolysis of Poly(ethylene terephthalate), *Macromolecules*, 2009, **42**, 5128-5138.
16. K. Shi, J. Jing, L. Song, T. Su and Z. Wang, Enzymatic hydrolysis of polyester: Degradation of poly(ε-caprolactone) by Candida antarctica lipase and Fusarium solani cutinase, *Int. J. Biol. Macromol.*, 2020, **144**, 183-189.
17. F. Kawai, U. Thumarat, K. Kitadokoro, T. Waku, T. Tada, N. Tanaka and T. Kawabata, in *Green Polymer Chemistry: Biocatalysis and Materials II*, American Chemical Society, 2013, vol. 1144, ch. 9, pp. 111-120.
18. C. M. Carr, D. J. Clarke and A. D. W. Dobson, Microbial Polyethylene Terephthalate Hydrolases: Current and Future Perspectives, *Frontiers in Microbiology*, 2020, **11**.
19. E. L. Bell, R. Smithson, S. Kilbride, J. Foster, F. J. Hardy, S. Ramachandran, A. A. Tedstone, S. J. Haigh, A. A. Garforth, P. J. R. Day, C. Levy, M. P. Shaver and A. P. Green, Directed evolution of an efficient and thermostable PET depolymerase, *Nat. Catal.*, 2022, **5**, 673-681.
20. A. Su, T. Tyrikos-Ergas, A. N. Shirke, Y. Zou, A. L. Dooley, I. V. Pavlidis and R. A. Gross, Revealing Cutinases' Capabilities as Enantioselective Catalysts, *ACS Catal.*, 2018, **8**, 7944-7951.
21. A. Mrigwani, M. Pitaliya, H. Kaur, B. Kasilingam, B. Thakur and P. Guptasarma, Rational mutagenesis of Thermobifida fusca cutinase to modulate the enzymatic degradation of polyethylene terephthalate, *Biotechnol. Bioeng.*, 2023, **120**, 674-686.

22. I. Kleeberg, K. Welzel, J. VandenHeuvel, R. J. Müller and W. D. Deckwer, Characterization of a New Extracellular Hydrolase from Thermobifida fusca Degrading Aliphatic–Aromatic Copolyesters, *Biomacromolecules*, 2005, **6**, 262-270.
23. Z. Zhang, S. Huang, D. Cai, C. Shao, C. Zhang, J. Zhou, Z. Cui, T. He, C. Chen, B. Chen and T. Tan, Depolymerization of post-consumer PET bottles with engineered cutinase 1 from Thermobifida cellulosilytica, *Green Chem.*, 2022, **24**, 5998-6007.
24. V. Tournier, C. M. Topham, A. Gilles, B. David, C. Folgoas, E. Moya-Leclair, E. Kamionka, M. L. Desrousseaux, H. Texier, S. Gavalda, M. Cot, E. Guémard, M. Dalibey, J. Nomme, G. Cioci, S. Barbe, M. Chateau, I. André, S. Duquesne and A. Marty, An engineered PET depolymerase to break down and recycle plastic bottles, *Nature*, 2020, **580**, 216-219.
25. I. Taniguchi, S. Yoshida, K. Hiraga, K. Miyamoto, Y. Kimura and K. Oda, Biodegradation of PET: Current Status and Application Aspects, *ACS Catal.*, 2019, **9**, 4089-4105.
26. A. Berselli, M. J. Ramos and M. C. Menziani, Novel Pet-Degrading Enzymes: Structure-Function from a Computational Perspective, *ChemBioChem*, 2021, **22**, 2032-2050.
27. R. Wei, G. von Haugwitz, L. Pfaff, J. Mican, C. P. S. Badenhorst, W. Liu, G. Weber, H. P. Austin, D. Bednar, J. Damborsky and U. T. Bornscheuer, Mechanism-Based Design of Efficient PET Hydrolases, *ACS Catal.*, 2022, **12**, 3382-3396.
28. H. Lu, D. J. Diaz, N. J. Czarnecki, C. Zhu, W. Kim, R. Shroff, D. J. Acosta, B. R. Alexander, H. O. Cole, Y. Zhang, N. A. Lynd, A. D. Ellington and H. S. Alper, Machine learning-aided engineering of hydrolases for PET depolymerization, *Nature*, 2022, **604**, 662-667.
29. Y. Cui, Y. Chen, X. Liu, S. Dong, Y. e. Tian, Y. Qiao, R. Mitra, J. Han, C. Li, X. Han, W. Liu, Q. Chen, W. Wei, X. Wang, W. Du, S. Tang, H. Xiang, H. Liu, Y. Liang, K. N. Houk and B. Wu, Computational Redesign of a PETase for Plastic Biodegradation under Ambient Condition by the GRAPE Strategy, *ACS Catal.*, 2021, **11**, 1340-1350.
30. L. Pfaff, J. Gao, Z. Li, A. Jäckering, G. Weber, J. Mican, Y. Chen, W. Dong, X. Han, C. G. Feiler, Y.-F. Ao, C. P. S. Badenhorst, D. Bednar, G. J. Palm, M. Lammers, J. Damborsky, B. Strodel, W. Liu, U. T. Bornscheuer and R. Wei, Multiple Substrate Binding Mode-Guided Engineering of a Thermophilic PET Hydrolase, *ACS Catal.*, 2022, **12**, 9790-9800.
31. H. F. Son, I. J. Cho, S. Joo, H. Seo, H.-Y. Sagong, S. Y. Choi, S. Y. Lee and K.-J. Kim, Rational Protein Engineering of Thermo-Stable PETase from Ideonella sakaiensis for Highly Efficient PET Degradation, *ACS Catal.*, 2019, **9**, 3519-3526.
32. B. Eiamthong, P. Meesawat, T. Wongsatit, J. Jitdee, R. Sangsri, M. Patchsung, K. Aphicho, S. Suraritdechachai, N. Huguenin-Dezot, S. Tang, W. Suginta, B. Paosawatyanyong, M. M. Babu, J. W. Chin, D. Pakotiprapha, W. Bhanthumnavin and C. Uttamapinant, Discovery and Genetic Code Expansion of a Polyethylene Terephthalate (PET) Hydrolase from the Human Saliva Metagenome for the Degradation and Bio-Functionalization of PET, *Angew. Chem. Int. Ed.*, 2022, **61**, e202203061.
33. K. Chen, Y. Hu, X. Dong and Y. Sun, Molecular Insights into the Enhanced Performance of EKylated PETase Toward PET Degradation, *ACS Catal.*, 2021, **11**, 7358-7370.
34. A. Nakamura, N. Kobayashi, N. Koga and R. Iino, Positive Charge Introduction on the Surface of Thermostabilized PET Hydrolase Facilitates PET Binding and Degradation, *ACS Catal.*, 2021, **11**, 8550-8564.
35. S. Brott, L. Pfaff, J. Schuricht, J.-N. Schwarz, D. Böttcher, C. P. S. Badenhorst, R. Wei and U. T. Bornscheuer, Engineering and evaluation of thermostable IsPETase variants for PET degradation, *Eng. Life Sci.*, 2022, **22**, 192-203.
36. W. Zeng, X. Li, Y. Yang, J. Min, J.-W. Huang, W. Liu, D. Niu, X. Yang, X. Han, L. Zhang, L. Dai, C.-C. Chen and R.-T. Guo, Substrate-Binding Mode of a Thermophilic PET Hydrolase and Engineering the Enzyme to Enhance the Hydrolytic Efficacy, *ACS Catal.*, 2022, **12**, 3033-3040.
37. U. Witt, R.-J. Müller and W.-D. Deckwer, Biodegradation behavior and material properties of aliphatic/aromatic polyesters of commercial importance, *Journal of environmental polymer degradation*, 1997, **5**, 81-89.
38. U. Witt, M. Yamamoto, U. Seeliger, R. J. Müller and V. Warzelhan, Biodegradable Polymeric Materials-Not the Origin but the Chemical Structure Determines Biodegradability, *Angew. Chem. Int. Ed.*, 1999, **38**, 1438-1442.
39. E. Marten, R.-J. Müller and W.-D. Deckwer, Studies on the enzymatic hydrolysis of polyesters I. Low molecular mass model esters and aliphatic polyesters, *Polym. Degrad. Stab.*, 2003, **80**, 485-501.
40. E. Marten, R.-J. Müller and W.-D. Deckwer, Studies on the enzymatic hydrolysis of polyesters. II. Aliphatic–aromatic copolyesters, *Polym. Degrad. Stab.*, 2005, **88**, 371-381.
41. I. Kleeberg, K. Welzel, J. Vandenheuvel, R. J. Müller and W. D. Deckwer, Characterization of a new extracellular hydrolase from Thermobifida fusca degrading aliphatic-aromatic copolyesters, *Biomacromolecules*, 2005, **6**, 262-270.
42. E. Herrero Acero, D. Ribitsch, A. Dellacher, S. Zitzenbacher, A. Marold, G. Steinkellner, K. Gruber, H. Schwab and G. M. Guebitz, Surface engineering of a cutinase from Thermobifida cellulosilytica for improved polyester hydrolysis, *Biotechnol. Bioeng.*, 2013, **110**, 2581-2590.
43. R. Wei and W. Zimmermann, Biocatalysis as a green route for recycling the recalcitrant plastic polyethylene terephthalate, *Microb. Biotechnol.*, 2017, **10**, 1302-1307.
44. R. Wei, T. Oeser, J. Then, N. Kühn, M. Barth, J. Schmidt and W. Zimmermann, Functional characterization and structural modeling of synthetic polyester-degrading hydrolases from Thermomonospora curvata, *AMB Express*, 2014, **4**, 44.
45. B. Liu, L. He, L. Wang, T. Li, C. Li, H. Liu, Y. Luo and R. Bao, Protein Crystallography and Site-Direct Mutagenesis Analysis of the Poly(ethylene terephthalate) Hydrolase PETase from Ideonella sakaiensis, *ChemBioChem*, 2018, **19**, 1471-1475.
46. Z. Chen, Y. Wang, Y. Cheng, X. Wang, S. Tong, H. Yang and Z. Wang, Efficient biodegradation of highly crystallized polyethylene terephthalate through cell surface display of bacterial PETase, *Sci. Total Environ.*, 2020, **709**, 136138.
47. S. Yoshida, K. Hiraga, T. Takehana, I. Taniguchi, H. Yamaji, Y. Maeda, K. Toyohara, K. Miyamoto, Y. Kimura and K. Oda, A bacterium that degrades and assimilates poly(ethylene terephthalate), *Science*, 2016, **351**, 1196-1199.

48. I. Roszak, L. Oswald, A. Al Ouahabi, A. Bertin, E. Laurent, O. Felix, I. Carvin-Sergent, L. Charles and J.-F. Lutz, Synthesis and sequencing of informational poly(amino phosphodiester)s, *Polymer Chemistry*, 2021, **12**, 5279-5282.
49. S. R. A. Molenaar, B. van de Put, J. S. Desport, S. Samanipour, R. A. H. Peters and B. W. J. Pirok, Automated Feature Mining for Two-Dimensional Liquid Chromatography Applied to Polymers Enabled by Mass Remainder Analysis, *Anal. Chem.*, 2022, **94**, 5599-5607.
50. K. M. Saller, I. Gnatiuk, D. Holzinger and C. Schwarzinger, Semiquantitative Approach for Polyester Characterization Using Matrix-Assisted Laser Desorption Ionization/Time-of-Flight Mass Spectrometry Approved by (1)H NMR, *Anal. Chem.*, 2020, **92**, 15221-15228.
51. J. S. Desport, G. Frache and L. Patiny, MSPolyCalc: A web-based App for polymer mass spectrometry data interpretation. The case study of a pharmaceutical excipient, *Rapid Commun. Mass Spectrom.*, 2020, **34**, e8652.
52. E. Krieger, G. Koraimann and G. Vriend, Increasing the precision of comparative models with YASARA NOVA--a self-parameterizing force field, *Proteins*, 2002, **47**, 393-402.
53. C. Oostenbrink, A. Villa, A. E. Mark and W. F. van Gunsteren, A biomolecular force field based on the free enthalpy of hydration and solvation: the GROMOS force-field parameter sets 53A5 and 53A6, *J. Comput. Chem.*, 2004, **25**, 1656-1676.